SAE 4140
((0.012 Max S) Steel
Iteration #76

Microstructural Data, Monotonic
And
Fatigue Test Results

Prepared by:

N. Cyril
and
A. Fatemi

Department of Mechanical, Industrial and
Manufacturing Engineering
The University of Toledo
Toledo, Ohio 43606

Prepared for:
The AISI Bar Steel Applications Group

October 2006

American Iron and Steel Institute

TABLE OF CONTENTS

UNIT CONVERSION TABLE

Measure	SI Unit	US Unit	from SI to US	from US to SI
Length	mm	in	$1 \text{ mm} = 0.03937 \text{ in}$	$1 \text{ in} = 25.4 \text{ mm}$
Area	mm^2	in^2	$1 \text{ mm}^2 = 0.00155 \text{ in}^2$	$1 \text{ in}^2 = 645.16 \text{ mm}^2$
Load	kN	klb	$1 kN = 0.2248 \text{ klb}$	$1 \text{ klb} = 4.448 \text{ kN}$
Stress	MPa	ksi	$1 \text{ MPa} = 0.14503 \text{ ksi}$	$1 \text{ ksi} = 6.895 \text{ MPa}$
Temperature	^{o}C	^{o}F	$^{o}C = (^{o}F - 32)/1.8$	$^{o}F = (^{o}C * 1.8) + 32$

In SI Unit:

$1 \text{ kN} = 10^3 \text{ N}$ $1 \text{ Pa} = 1 \text{ N/m}^2$ $1 \text{ MPa} = 10^6 \text{ Pa} = 1 \text{ N/mm}^2$ $1 \text{ Gpa} = 10^9 \text{ Pa}$

In US Unit:

$1 \text{ klb} = 10^3 \text{ lb}$ $1 \text{ psi} = 1 \text{ lb/in}^2$ $1 \text{ ksi} = 10^3 \text{ psi}$

NOMENCLATURE

A_o, A_f	initial, final area	S	engineering stress
HB, HRB, HRC	Brinell, Rockwell B-Scale, Rockwell C-Scale hardness number	YS, UYS, LYS, YS'	monotonic yield, upper yield, lower yield, cyclic yield strength
b, c, n	fatigue strength, fatigue ductility, strain hardening exponent	YPE	yield point elongation
D_o, D_f	initial, final diameter	S_u	ultimate tensile strength
e	engineering strain	%EL	percent elongation
E, E'	monotonic, midlife cycle modulus of elasticity	%RA	percent reduction in area
K, K'	monotonic, cyclic strength coefficient	σ, σ_f, σ_f'	true stress, true fracture strength, fatigue strength coefficient
L_o, L_f	initial, final gage length	σ_a, σ_m, $\Delta\sigma$	stress amplitude, mean stress, stress range
$N_{50\%}$, $(N_f)_{10\%}$, $(N_f)_{50\%}$,	number of cycles to midlife, 10% load drop, 50% load drop	ε_e, ε_p, ε	true elastic, plastic, total strain
$2N_f$	reversals to failure	ε_f, ε_f'	true fracture ductility, fatigue ductility coefficient
P_f, P_u	fracture, ultimate load	ε_a, ε_m, $\Delta\varepsilon$	strain amplitude, mean strain, strain range
R	neck radius; or strain ratio	$\Delta\varepsilon_e$, $\Delta\varepsilon_p$	elastic, plastic strain range

SUMMARY

The microstructural data, monotonic properties, and fatigue behavior data have been obtained for SAE 4140 Low S (0.012% max) quenched and tempered steel. The material was provided for the American Iron and Steel Institute (AISI) by Macsteel Company – Monroe Division. Microstructural data includes grain type, grain size, and inclusion content. Two tensile tests were performed to acquire the desired monotonic properties. Twenty strain-controlled fatigue tests were performed to obtain the strain-life and cyclic stress-strain curves and properties. The experimental procedure followed and results obtained are presented and discussed in this report.

I. EXPERIMENTAL PROGRAM

1.1 Material and Specimen Fabrication

1.1.1 Material

The SAE 4140 Low S (0.012% max S) quenched and tempered steel was provided by Macsteel Company – Monroe Division. 6" square continuous cast billets were forged into 2.5" square from which 0.625" wide slabs were cut lengthwise at Macsteel Company. Then coupons of 0.625" wide slices in the transverse direction were cut from them at Macsteel. The specimens were then machined from rectangular 0.625"x0.625"x2.5" coupons at the University of Toledo. In Table 1, the chemical composition supplied by Macsteel Company is shown. Figures 1b, 1c and 1d show the sample arrangement for testing of transverse properties and the sulfur printing of this material also provided by Macsteel Company.

1.1.2 Specimen

In this study, identical round specimens were used for the monotonic and fatigue tests. The specimen configuration and dimensions are shown in Figure 1a. This configuration deviates slightly from the specimens recommended by ASTM Standard E606 [1]. The recommended specimens have uniform or hourglass test sections. The specimen geometry shown in Figure 1 differs by using a large secondary radius throughout the test section. In addition, the grip sections are short due to maximum available length of 2.5" from the forged square section.

All specimens were machined in the Mechanical, Industrial, and Manufacturing Engineering Machine Shop at the University of Toledo. The specimens were initially turned on a lathe to an appropriate diameter for insertion into a CNC machine. Using the CNC machine, final turning was performed to achieve the tolerable dimensions specified on the specimen drawings.

The specimens were then heat treated at Daimler Chrysler, after which they were ground at Metal Samples Inc. These specimens were then polished prior to testing at the University of Toledo. A commercial round-specimen polishing machine was used to polish the specimen gage section. Three different grits of aluminum oxide lapping film were used: 30μ, 15μ, and 3μ. The 3μ grit was used as the final polish and polishing marks coincided with the specimens' longitudinal direction. The polished surfaces were carefully examined under magnification to ensure complete removal of machine marks within the test section.

1.2 Testing Equipment

1.2.1 Apparatus

An INSTRON 8801 closed-loop servo-controlled hydraulic axial load frame in conjunction with a Fast-Track digital servo-controller was used to conduct the tests. The calibration of this system was verified prior to beginning the test program. The load cell used had a capacity of 50 kN. Hydraulically operated grips using universal tapered collets were employed to secure the specimens' ends in series with the load cell.

Total strain was controlled for all tests using an extensometer rated as ASTM class B1 [2]. The calibration of the extensometer was verified using displacement apparatus

3

containing a micrometer barrel in divisions of 0.0001 in. The extensometer had a gage length of 0.30 in and was capable of measuring strains up to 15 %.

In order to protect the specimens' surface from the knife-edges of the extensometer, ASTM Standard E606 recommends the use of transparent tape or epoxy to 'cushion' the attachment. For this study, it was found that application of transparent tape strips was difficult due to the radius within the test section. Therefore, epoxy was considered to be the best protection. One disadvantage of epoxy is the variability of mixtures throughout the test program. As an alternative to epoxy, M-coat D offered a more consistent mixture. Therefore, the tests were performed using M-coat D.

All tests were conducted at room temperature and were monitored using a digital thermometer. In order to minimize temperature effects upon the extensometer and load cell calibrations, fluctuations were maintained within ± 2 °C (± 3.6 °F) as required by ASTM Standard E606. Also, the relative humidity of the air was monitored using a precision hydrometer.

1.2.2 Alignment

Significant effort was put forth to align the load train (load cell, grips, specimen, and actuator). Misalignment can result from both tilt and offset between the central lines of the load train components. According to ASTM Standard E606, the maximum bending strains should not exceed 5 % of the minimum axial strain range imposed during any test program. For this study, the minimum axial strain range was 0.0055 in/in, which was used in the run-out fatigue test. Therefore, the maximum allowable bending strain was 275 microstrain. ASTM Standard E1012, Type A, Method 1 was followed to verify specimen

alignment [3]. For this procedure, two arrays of four strain gages per array were arranged at the upper and lower ends of the uniform gage section. For each array, gages were equally spaced around the circumference of a 0.5-in. diameter specimen with uniform gage section. The maximum bending strain determined from the gaged specimen was within the allowable ASTM limit.

1.3 Test Methods and Procedures

1.3.1 Monotonic tension tests

All monotonic tests in this study were performed using test methods specified by ASTM Standard E8 [4]. Two specimens were used to obtain the monotonic properties. In order to protect the extensometer, strain control was used only up to 5.1% strain, until the point of ultimate tensile strength had been crossed. After this point, displacement control was used until fracture.

For the elastic and initial yield region (0% to 0.5% strain), a strain rate of 0.0025 in/in/min was chosen. This strain rate was three-quarters of the maximum allowable rate specified by ASTM Standard E8 for the initial yield region. After yielding (0.5% to 5.1% strain), the strain rate was increased by a factor of three (i.e., 0.0075 in/in/min). After the extensometer was removed, a displacement rate of 0.006 in/min was used. This displacement rate provided approximately the same strain rate as that used prior to switching control modes.

After the tension tests were concluded, the broken specimens were carefully reassembled. The final gage lengths of the fractured specimens were measured with a

Vernier caliper having divisions of 0.001 in. Using an optical comparator with 10X magnification and divisions of 0.001 in, the final diameter and the neck radius were measured. It should be noted that prior to the test, the initial minimum diameter was measured with this same instrument.

1.3.2 Constant amplitude fatigue tests

All constant amplitude fatigue tests in this study were performed according to ASTM Standard E606. It is recommended by this standard that at least 10 specimens be used to generate the fatigue properties. For this study, 20 specimens at 7 different strain amplitudes ranging from 0.275% to 2% were utilized. INSTRON LCF software was used in all strain-controlled tests. During each strain-controlled test, the total strain was recorded using the extensometer output. Test data were automatically recorded throughout each test.

There were two control modes used for these tests. Strain control was used in all tests with plastic deformation. For some of the elastic tests, strain control was used initially to determine the stabilized load, then load control was used for the remainder of the test and for the rest of the elastic tests, load control was used throughout. The reason for the change in control mode was due to the frequency limitation on the extensometer. Load control was also used when the mean load shifted to a value higher than 10% of the stabilized load during a strain controlled test. For the strain control tests, the applied frequencies ranged from 0.2 Hz to 0.5 Hz in order to keep a strain rate about 0.02 in/in/sec. For the load-controlled tests, load waveforms with frequencies of up to 20 Hz were used in order to shorten the overall test duration. All tests were conducted using a triangular waveform.

II. Experimental results and analysis

2.1 Microstructural Data

Photomicrographs of the microstructure were obtained using an optical microscope with a digital camera attachment. Figure 1c indicates the L, T and T' directions. It was observed that the grains in the first longitudinal (L-T) and the second longitudinal (L-T') directions had negligible difference. In Figures 2a and 2b, the transverse (T-T') direction and the longitudinal (L-T) direction are shown at 500X magnification respectively. It can be seen from these photomicrographs that SAE 4140 Low S (0.012% max.) quenched and tempered steel had a martensite microstructure in both T-T' and L-T' directions. In Figure 3, the inclusions in the T-T' direction are shown at 100X magnification. (Provided by Macsteel Company)

The average grain size was measured in both transverse and longitudinal directions using the Linear Intercept Procedures reported in ASTM Standard E112 [5]. Rockwell hardness tests were also performed. A summary of the microstructural data for SAE 4140 Low S (0.012% max.) quenched and tempered steel is provided in Table 2.

2.2 Monotonic Deformation Behavior

The properties determined from monotonic tests were the following: modulus of elasticity (E), yield strength (YS), ultimate tensile strength (S_u), percent elongation (%EL), percent reduction in area (%RA), true fracture strength (σ_f), true fracture ductility (ε_f), strength coefficient (K), and strain hardening exponent (n).

True stress (σ), true strain (ε), and true plastic strain (ε_p) were calculated from engineering stress (S) and engineering strain (e), according to the following relationships which are based on constant volume assumption:

$$\sigma = S(1 + e) \tag{1a}$$

$$\varepsilon = \ln(1 + e) \tag{1b}$$

$$\varepsilon_p = \varepsilon - \varepsilon_e = \varepsilon - \frac{\sigma}{E} \tag{1c}$$

The true stress (σ) - true strain (ε) plot is often represented by the Ramberg-Osgood equation:

$$\varepsilon = \varepsilon_e + \varepsilon_p = \frac{\sigma}{E} + \left(\frac{\sigma}{K} \right)^{\frac{1}{n}} \tag{2}$$

The strength coefficient, K, and strain hardening exponent, n, are the intercept and slope of the best line fit to true stress (σ) versus true plastic strain (ε_p) data in log-log scale:

$$\sigma = K \left(\varepsilon_p \right)^n \tag{3}$$

In accordance with ASTM Standard E739 [7], when performing the least squares fit, the true plastic strain (ε_p) was the independent variable and the stress (σ) was the dependent variable. These plots for the two tests conducted are shown in Figure 4. To generate the K

and n values, the range of data used in this figure was chosen according to the definition of discontinuous yielding specified in ASTM Standard E646 [8]. Therefore, the valid data range occurred between the end of yield point extension and the strain at or prior to maximum load.

The true fracture strength, σ_f, was corrected for necking according to the Bridgman correction factor [9]:

$$\sigma_f = \frac{\dfrac{P_f}{A_f}}{\left[1 + \dfrac{4R}{D_f}\right] \ln\left[1 + \dfrac{D_f}{4R}\right]} \tag{4}$$

where P_f is the load at fracture, R is the neck radius, and D_f is the diameter at fracture.

The true fracture ductility, ε_f, was calculated from the relationship based on constant volume:

$$\varepsilon_f = \ln\left(\frac{A_o}{A_f}\right) = \ln\left(\frac{1}{1 - RA}\right) \tag{5}$$

where A_f is the cross-sectional area at fracture, A_o is the original cross-sectional area, and RA is the reduction in area.

A summary of the monotonic properties for SAE 4140 Low S (0.012% max.) quenched and tempered steel is provided in Table 2. The monotonic stress-strain curves are shown in Figure 5. As can be seen from this figure, the two curves are very close to each other. Refer to Table A.1 in the Appendix for a summary of the monotonic test results.

2.3 Cyclic Deformation Behavior

2.3.1 Transient cyclic response

Transient cyclic response describes the process of cyclic-induced change in deformation resistance of a material. Data obtained from constant amplitude strain-controlled fatigue tests were used to determine this response. Plots of stress amplitude variation versus applied number of cycles can indicate the degree of transient cyclic softening/hardening. Also, these plots show when cyclic stabilization occurs. A composite plot of the transient cyclic response for SAE 4140 Low S (0.012% max.) quenched and tempered steel is shown in Figure A.1 of the Appendix. The transient response was normalized on the rectangular plot in Figure A.1a, while a semi-log plot is shown in Figure A.1b. Even though multiple tests were conducted at each strain amplitude, data from one test at each strain amplitude tested are shown in these plots.

2.3.2 Steady-state cyclic deformation

Another cyclic behavior of interest was the steady state or stable response. Data obtained from constant amplitude strain-controlled fatigue tests were also used to determine this response. The properties determined from the steady-state hysteresis loops were the following: cyclic modulus of elasticity (E'), cyclic strength coefficient (K'), cyclic strain hardening exponent (n'), and cyclic yield strength (YS'). Half-life (midlife) hysteresis loops and data were used to obtain the stable cyclic properties.

Similar to monotonic behavior, the cyclic true stress-strain behavior can be characterized by the Ramberg-Osgood type equation:

$$\frac{\Delta \varepsilon}{2} = \frac{\Delta \varepsilon_e}{2} + \frac{\Delta \varepsilon_p}{2} = \frac{\Delta \sigma}{2E} + \left(\frac{\Delta \sigma}{2K'} \right)^{\frac{1}{n'}} \tag{6}$$

It should be noted that in Equation 6 and the other equations that follow, E is the average modulus of elasticity that was calculated from the monotonic tests.

The cyclic strength coefficient, K', and cyclic strain hardening exponent, n', are the intercept and slope of the best line fit to true stress amplitude ($\Delta\sigma/2$) versus true plastic strain amplitude ($\Delta\varepsilon_p/2$) data in log-log scale:

$$\frac{\Delta \sigma}{2} = K' \left(\frac{\Delta \varepsilon_p}{2} \right)^{n'} \tag{7}$$

In accordance with ASTM Standard E739, when performing the least squares fit, the true plastic strain amplitude ($\Delta\varepsilon_p/2$) was the independent variable and the stress amplitude ($\Delta\sigma/2$) was the dependent variable. The true plastic strain amplitude was calculated by the following equation:

$$\frac{\Delta \varepsilon_p}{2} = \frac{\Delta \varepsilon}{2} - \frac{\Delta \sigma}{2E} \tag{8}$$

This plot is shown in Figure 6. To generate the K' and n' values, the range of data used in this figure was chosen for $\left[\frac{\Delta \varepsilon_p}{2} \right]_{calculated} \geq 0.00020$ in/in.

The cyclic stress - strain curve reflects the resistance of a material to cyclic deformation and can be vastly different from the monotonic stress - strain curve. The cyclic stress - strain curve is shown in Figure 7. In Figure 8, superimposed plots of monotonic and cyclic curves are shown. As can be seen in Figure 8, SAE 4140 Low S (0.012% max.) quenched and tempered steel cyclically softens. Figure A.2 in the Appendix shows a

composite plot of the steady-state (midlife) hysteresis loops. Even though multiple tests were conducted at each strain amplitude, the stable loops from only one test at each strain amplitude are shown in this plot.

2.4 Constant Amplitude Fatigue Behavior

Constant amplitude strain-controlled fatigue tests were performed to determine the strain-life curve. The following equation relates the true strain amplitude to the fatigue life:

$$\frac{\Delta \varepsilon}{2} = \frac{\Delta \varepsilon_e}{2} + \frac{\Delta \varepsilon_p}{2} = \frac{\sigma_f'}{E}\left(2N_f\right)^b + \varepsilon_f'\left(2N_f\right)^c \tag{9}$$

where σ_f' is the fatigue strength coefficient, b is the fatigue strength exponent, ε_f' is the fatigue ductility coefficient, c is the fatigue ductility exponent, E is the monotonic modulus of elasticity, and $2N_f$ is the number of reversals to failure (which was defined as a 50% load drop, as recommended by ASTM Standard E606).

The fatigue strength coefficient, σ_f', and fatigue strength exponent, b, are the intercept and slope of the best line fit to true stress amplitude ($\Delta\sigma/2$) versus reversals to failure ($2N_f$) data in log-log scale:

$$\frac{\Delta \sigma}{2} = \sigma_f'\left(2N_f\right)^b \tag{10}$$

In accordance with ASTM Standard E739, when performing the least squares fit, the stress amplitude ($\Delta\sigma/2$) was the independent variable and the reversals to failure ($2N_f$) was the dependent variable. This plot is shown in Figure 9. To generate the σ_f' and b values, the range of data used in this figure was chosen for $N_f \leq 5 \times 10^6$ cycles.

The fatigue ductility coefficient, ε_f', and fatigue ductility exponent, c, are the intercept and slope of the best line fit to calculated true plastic strain amplitude ($\Delta\varepsilon_p/2$) versus reversals to failure ($2N_f$) data in log-log scale:

$$\left(\frac{\Delta\varepsilon_p}{2}\right)_{calculated} = \varepsilon_f'\left(2N_f\right)^C \qquad (11)$$

In accordance with ASTM Standard E739, when performing the least squares fit, the calculated true plastic strain amplitude ($\Delta\varepsilon_p/2$) was the independent variable and the reversals to failure ($2N_f$) was the dependent variable. The calculated true plastic strain amplitude was determined from Equation 8. This plot is shown in Figure 10. To generate the ε_f' and c values, the range of data used in this figure was chosen for $\left[\dfrac{\Delta\varepsilon_p}{2}\right]_{calculated} \geq$ 0.0002 in/in.

The true strain amplitude versus reversals to failure plot is shown in Figure 11. This plot displays the strain - life curve (Eqn. 9), the elastic strain portion (Eqn. 10), the plastic strain portion (Eqn. 11), and superimposed fatigue data.

A parameter often used to characterize fatigue behavior at stress concentrations, such as the root of a notch, is Neuber's parameter [10]. Neuber's stress range is given by:

$$\sqrt{(\Delta\varepsilon)\,(\Delta\sigma)\,E} = 2\sqrt{(\sigma_f')^2\,(2N_f)^{2b} + \sigma_f'\varepsilon_f'E\,(2N_f)^{b+c}} \qquad (12)$$

Plot of Neuber stress range versus reversals to failure is shown in figure12. this figure displays the Neuber curve based on Eqn. 12 and superimposed fatigue data for this material.

A summary of the cyclic properties for SAE 4140 Low S (0.012% max.) steel is provided in Table 2. Table A.2 in the Appendix provides the summary of the fatigue test results.

Table 1: Chemical composition of SAE 4140 (0.012 max S) steel

Element	Wt. %
Carbon, C	0.412%
Manganese, Mn	0.940%
Phosphorus, P	0.010%
Sulfur, S	0.012%
Silicon, Si	0.280%
Nitrogen, N	0.0094%
Chromium, Cr	1.010%
Aluminum, Al	0.028%
Nickel, Ni	0.15%
Molybdenum, Mo	0.220%
Copper, Cu	0.170%
Tin, Sn	0.007%
Dl	6.400%
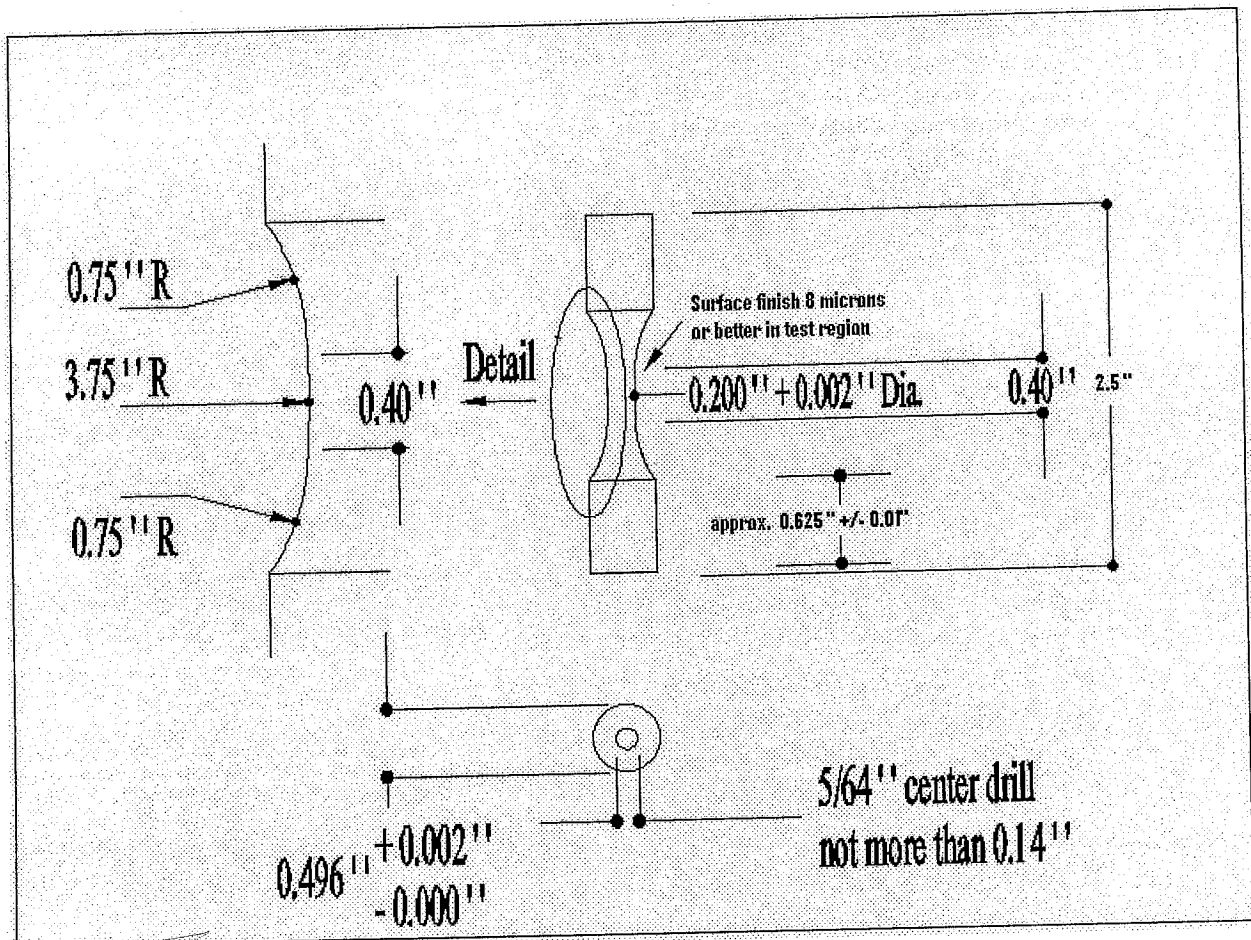
Figure 1a: Specimen configuration and dimensions

Table 2: Summary of the Mechanical Properties

Microstructural Data	Average
ASTM grain size number (MAG=500X):	
Transverse direction (T-T')	10 to 11
The longitudinal direction (L-T)(as shown in Fig. 1c)	11 to 12
Inclusion rating number (MAG=100X): (Provided by Macsteel Company)	
Type A (sulfide type), thin series	Thin:0.5,heavy:0
Type B (alumina type), thin & heavy series	None
Type C (silicate type), thin & heavy series	None
Type D (globular type), thin & heavy series	Heavy:1.0
Hardness:	
Brinell (HB)	
Transverse direction (T-T')	477 at center and 495 near surface(converted from HRC)
The first longitudinal direction (L-T)	-
Rockwell B-scale (HRB)	
Transverse direction (T-T')	-
The first longitudinal direction (L-T)	-
Rockwell C-scale (HRC)	
Transverse direction (T-T')	49.5 at the centre of gage and 51 near the surface (measured)
The first longitudinal direction (L-T)	-
Microstructure type:	
Transverse direction (T-T')	martensite
The first longitudinal direction (L-T)	martensite

Monotonic Properties	Average		Range	
Modulus of elasticity, E, GPa (ksi):	213.0	(30,890.5)	207.2 - 218.8	(30,053.7 - 31,727.3)
Yield strength (0.2% offset), YS , MPa (ksi):	1669.2	(242.1)	1658.1 - 1680.3	(240.5 - 243.7)
Upper yield strength UYS, MPa (ksi):	-	-	- - -	- - -
Lower yield strength LYS, MPa (ksi):	-	-	- - -	- - -
Yield point elongation, YPE (%):	-	-	- - -	- -
Ultimate strength, S_u , MPa (ksi):	1924.3	(279.1)	1916.0 - 1932.7	(277.9 - 280.3)
Percent elongation, %EL (%):	8.5%		3.7% - 13.3%	
Percent reduction in area, %RA (%):	15.7%		6.9% - 24.4%	
Strength coefficient, K , MPa (ksi):	2,625.9	(380.8)	2,601.6 - 2,650.1	(377.3 - 384.4)
Strain hardening exponent, n:	0.0710		0.0708 - 0.0712	
True fracture strength, σ_f , MPa (ksi):	1859.0	(282.1)	1855.2 - 1862.8	(269.1 - 295.2)
True fracture ductility, ε_f (%):	16.3%		6.9% - 25.7%	

| Cyclic Properties	Average		Range	
Cyclic modulus of elasticity, E' , GPa (ksi):	198.1	(28,728.2)	186.9 - 210.4	(27,109.0) - (30,517.5)
Fatigue strength coefficient, σ_f' , MPa (ksi):	2,785	(403.9)		
Fatigue strength exponent, b:	-0.1072			
Fatigue ductility coefficient, ε_f' :	0.22054			
Fatigue ductility exponent, c:	-0.7118			
Cyclic strength coefficient, K' , MPa (ksi):	2,722.1	(394.8)		
Cyclic strain hardening exponent, n':	0.1068			
Cyclic yield strength, YS', MPa (ksi)	1401.7	(203.3)		
Fatigue Limit (defined at 10^6 cycles), Mpa (ksi)	587.72	(85.2)		
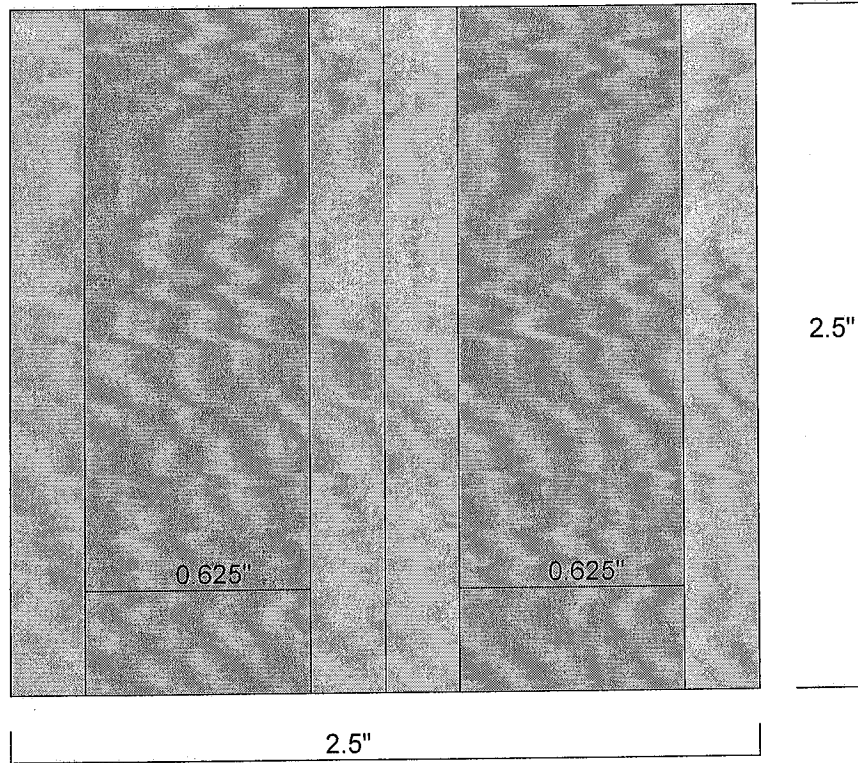
Figure 1b: Sample arrangement for testing of transverse properties in 4140 steels. (provided by Macsteel Company – Monroe Division)
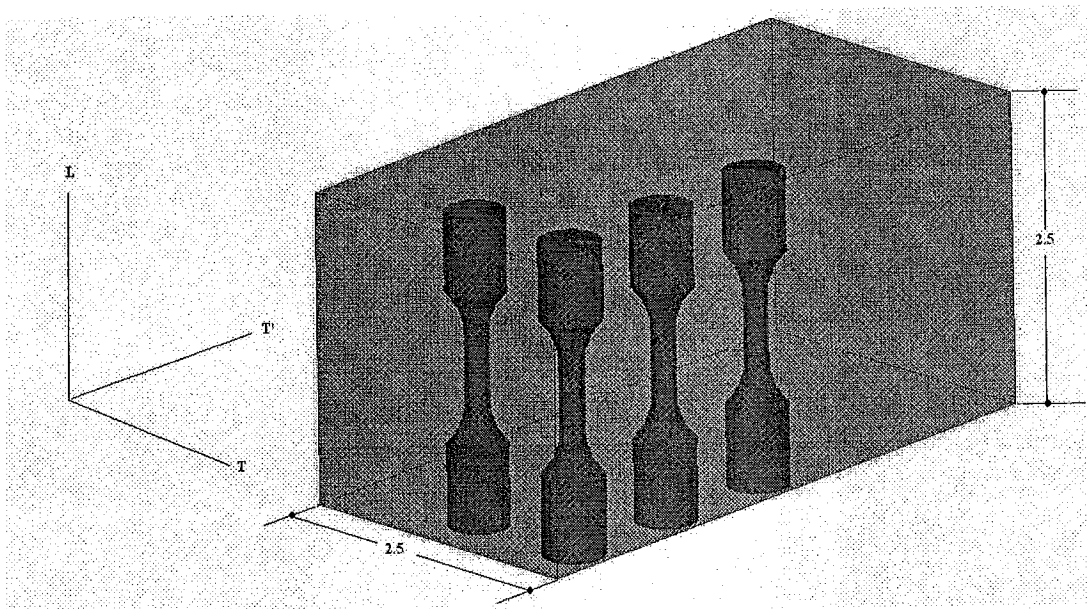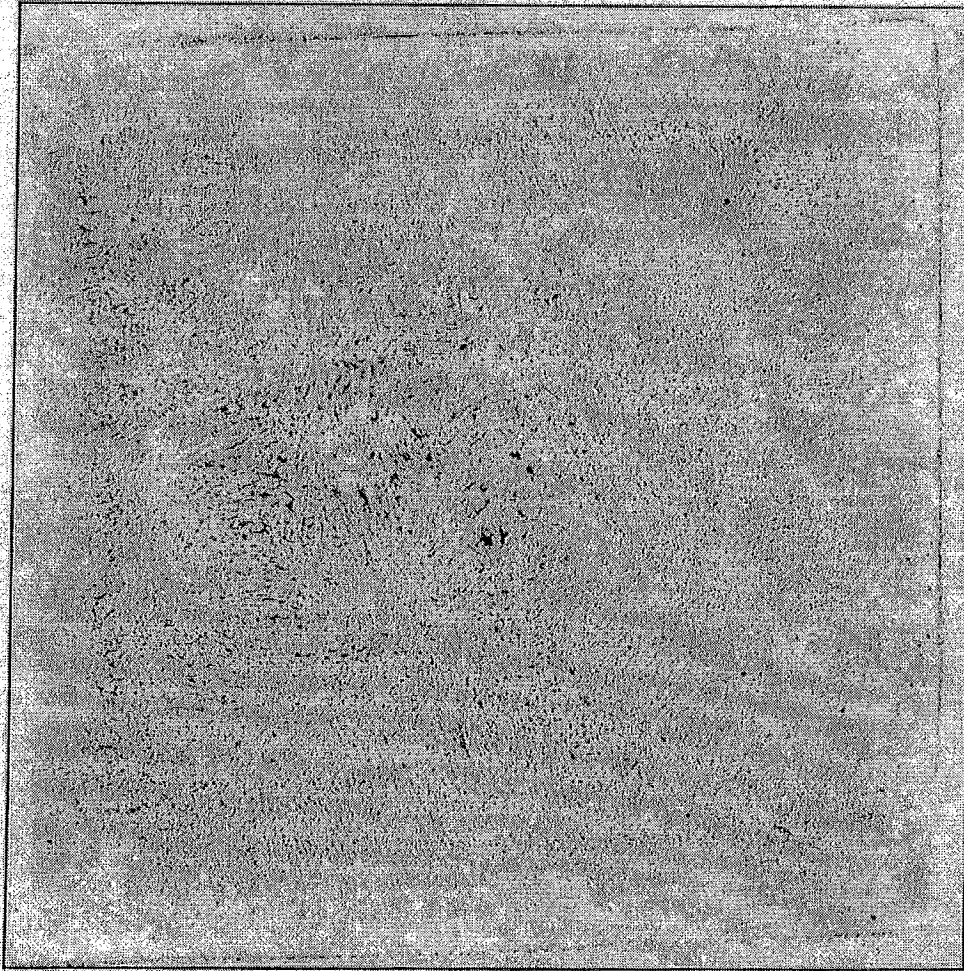

Figure 1c: Sample cut-out direction

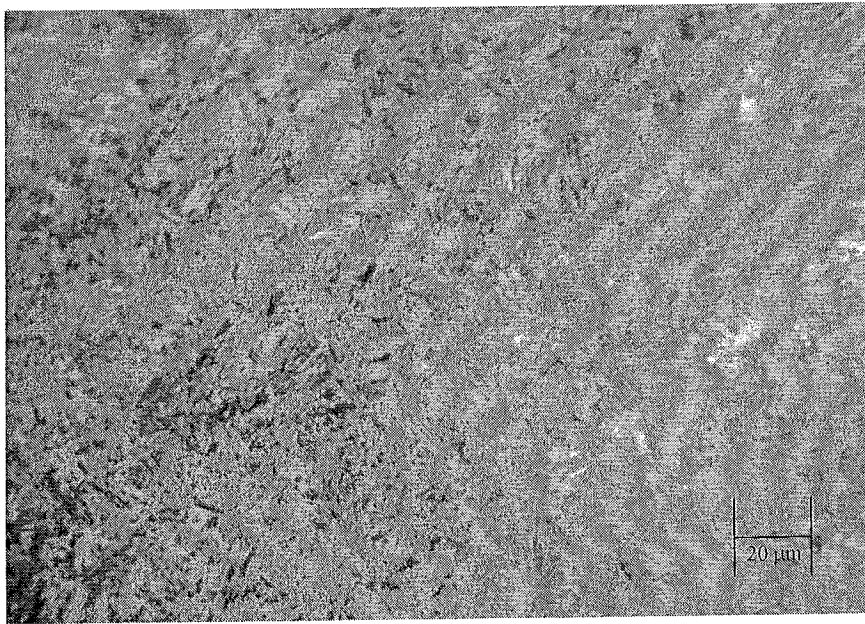Figure 1d: Sulfur printing of heat no.17300 (It 76)(Provided by Macsteel – Monroe Division)

Figure 2a: Photomicrograph in the transverse direction (T-T' as shown in Fig. 1c) at 500X for SAE 4140 Low S (0.012% max.) steel.
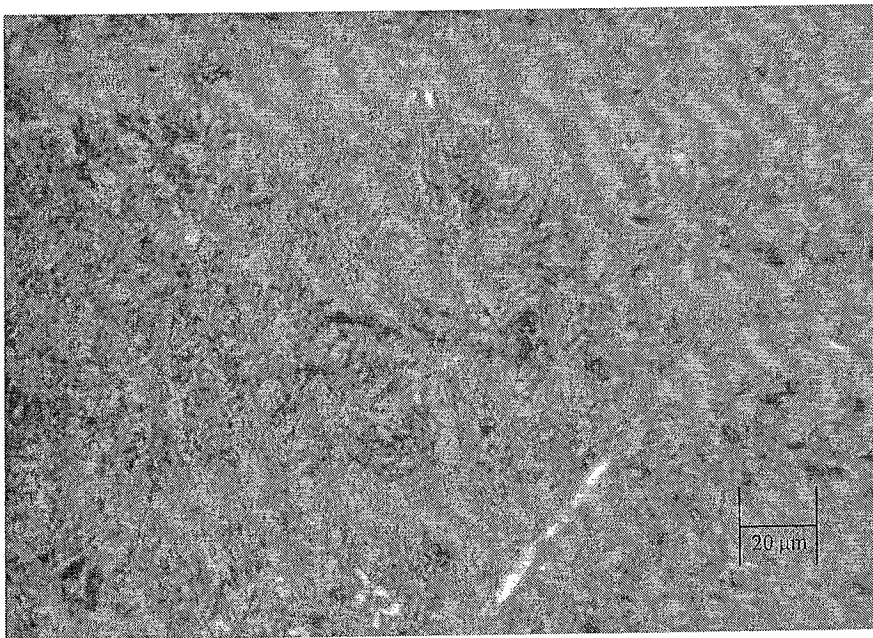

Figure 2b: Photomicrograph in the longitudinal direction (L-T as shown in Fig. 1c) at 500X for SAE 4140 Low S (0.012% max.) steel.
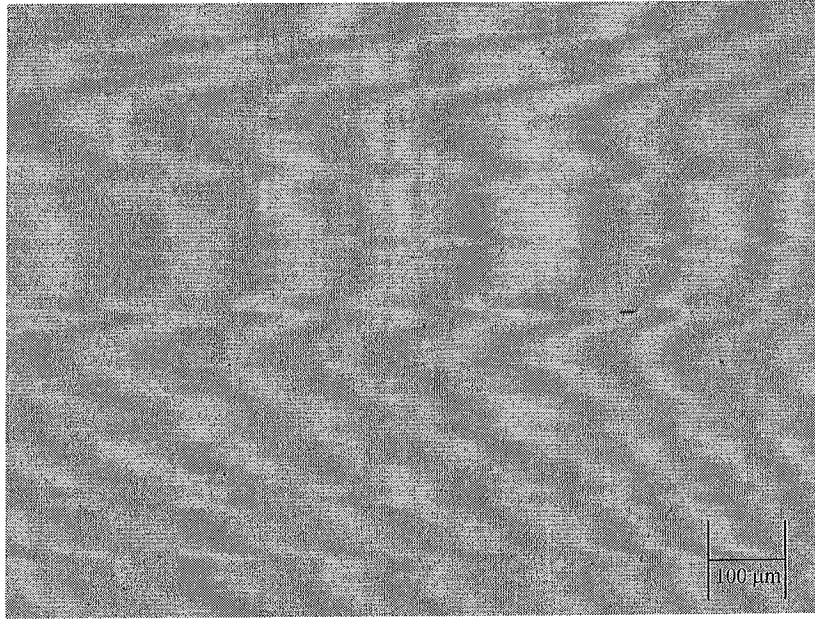
19

Figure 3: Sulfide Inclusions in 2.5" square bars Heat M17300 – 0.012% S
(original 100X) Rated as A thin = 0.5 and A heavy = 0, D thin = 1.0 and D heavy = 1.0
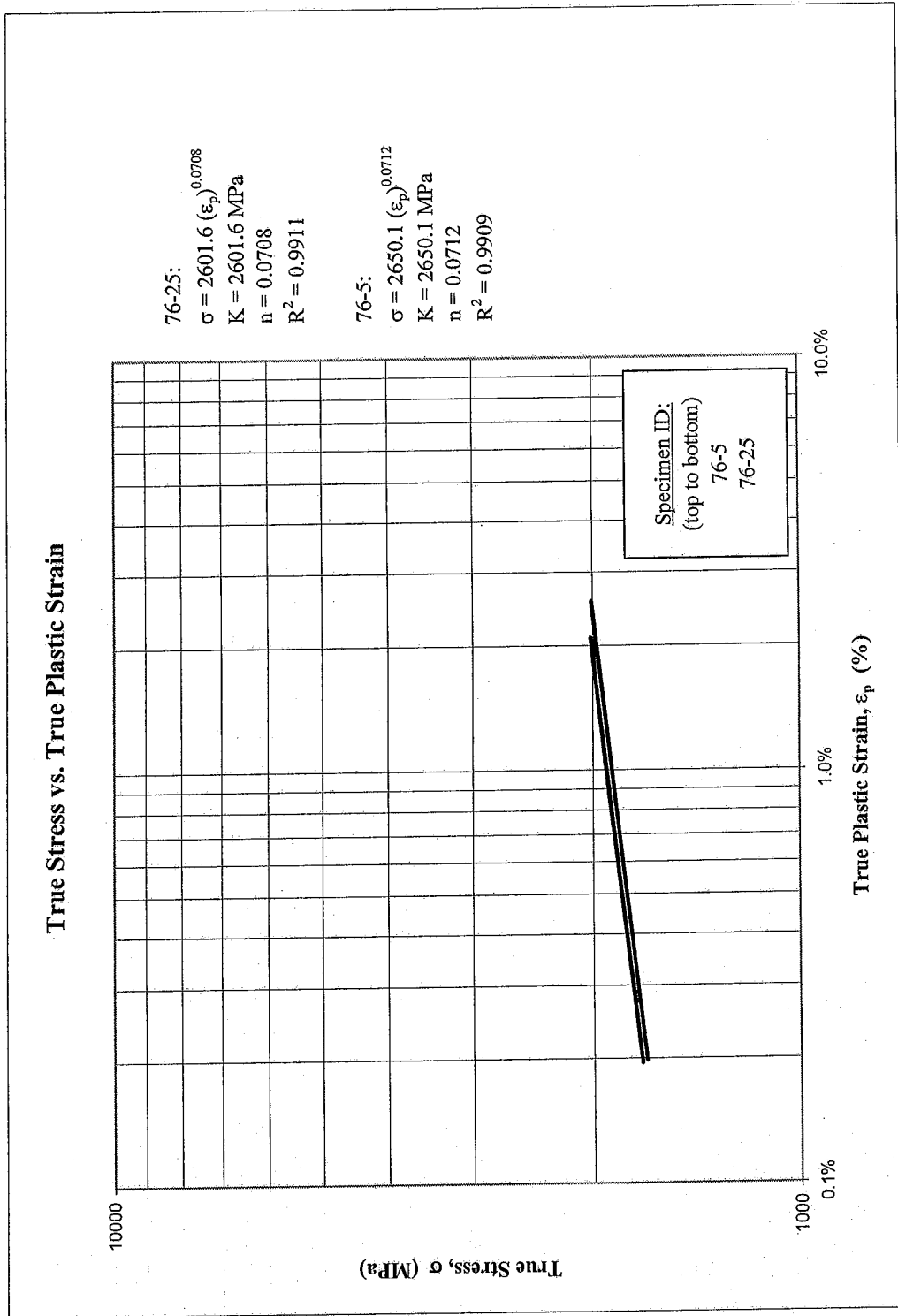(no B or C) (Provided by Macsteel Company – Monroe Division)

True Stress vs. True Plastic Strain

76-25:
$\sigma = 2601.6\,(\varepsilon_p)^{0.0708}$
$K = 2601.6$ MPa
$n = 0.0708$
$R^2 = 0.9911$

76-5:
$\sigma = 2650.1\,(\varepsilon_p)^{0.0712}$
$K = 2650.1$ MPa
$n = 0.0712$
$R^2 = 0.9909$

Specimen ID:
(top to bottom)
76-5
76-25

True Stress, σ (MPa)

True Plastic Strain, ε_p (%)

10000

1000

0.1%   1.0%   10.0%

Figure 4: True stress versus true plastic strain

Engineering Stress vs. Engineering Strain

Specimen ID:
(top to bottom)
76-5
76-25

Engineering Strain, e (%)

Engineering Stress, S (MPa)
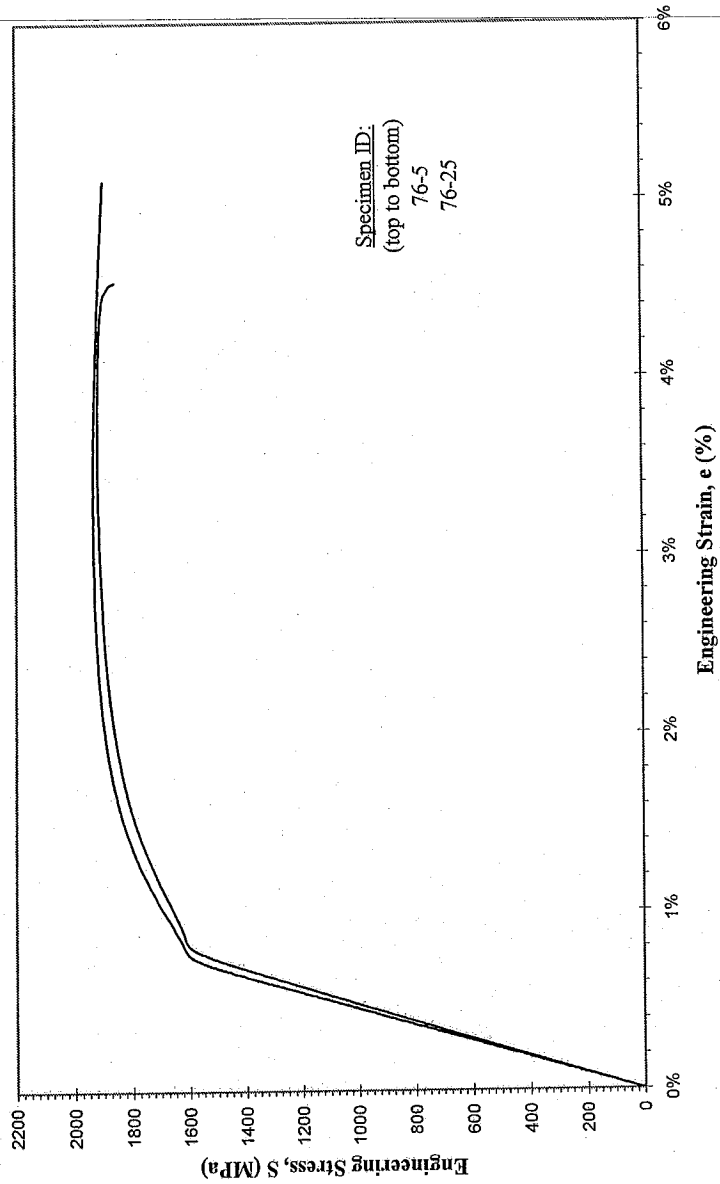
Figure 5: Monotonic stress-strain curve

True Stress Amplitude vs. True Plastic Strain Amplitude (Calculated)

$\Delta\sigma/2 = 2722.1(\Delta\varepsilon_p/2)^{0.1068}$
K ' = 2722.1 MPa
n ' = 0.1068
R^2 = 0.9637

○ Data
—— Power (Data)

10000

True Stress Amplitude, Δσ/2 (MPa)

1000

0.01%   0.10%   1.00%   10.00%

True Plastic Strain Amplitude, Δε_p/2 (%)
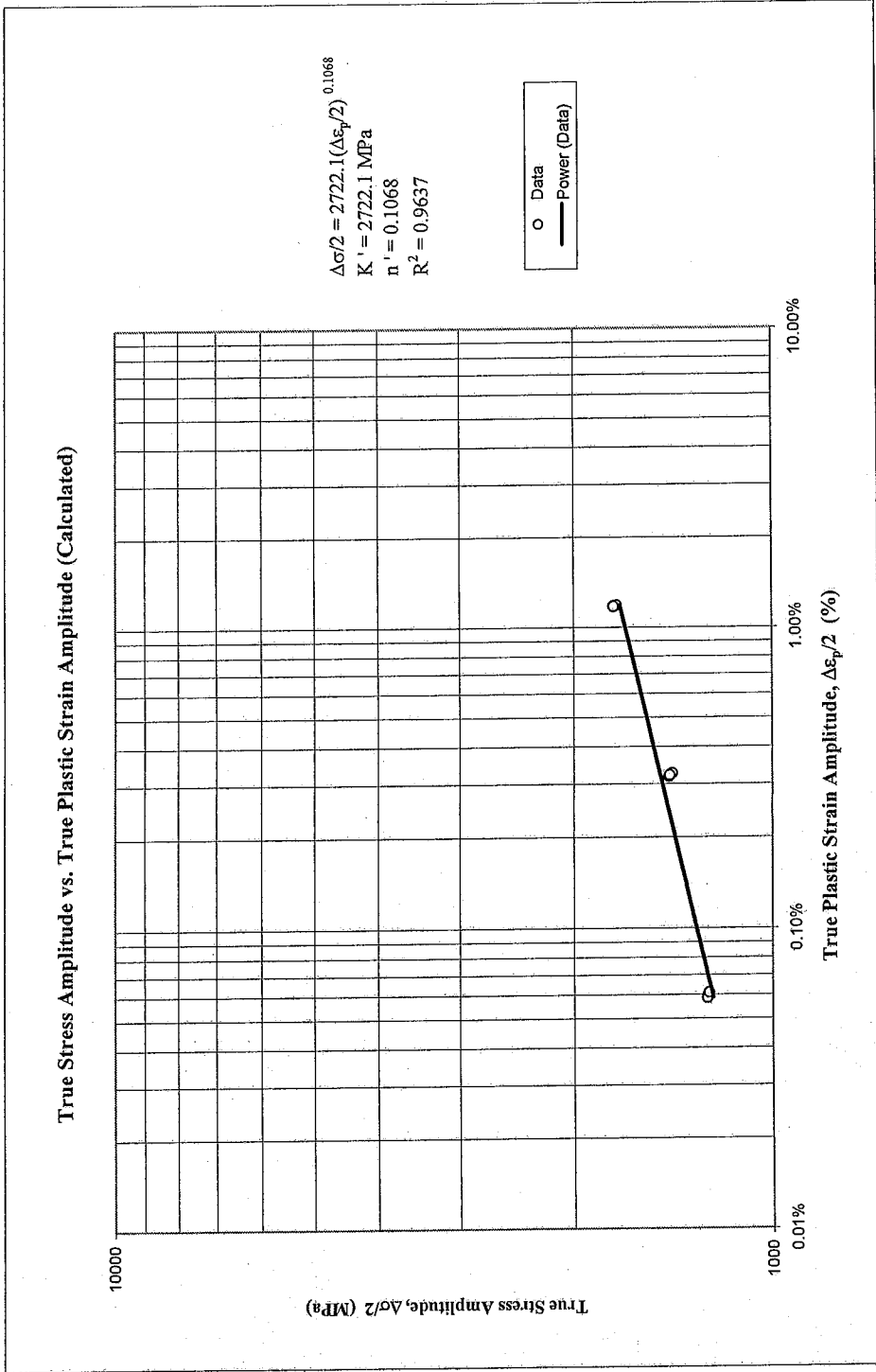
Figure 6: True stress amplitude versus calculated true plastic strain amplitude
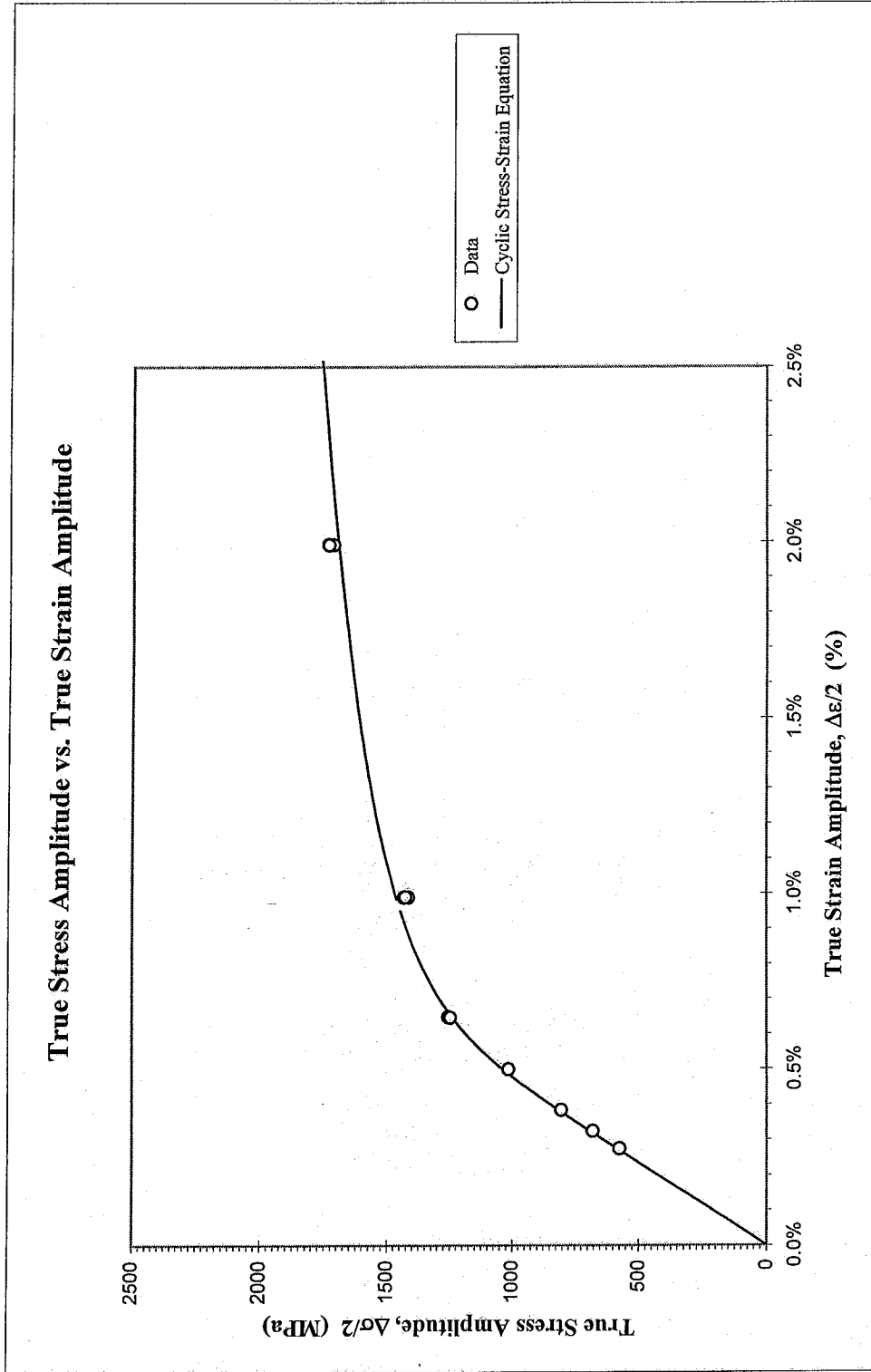
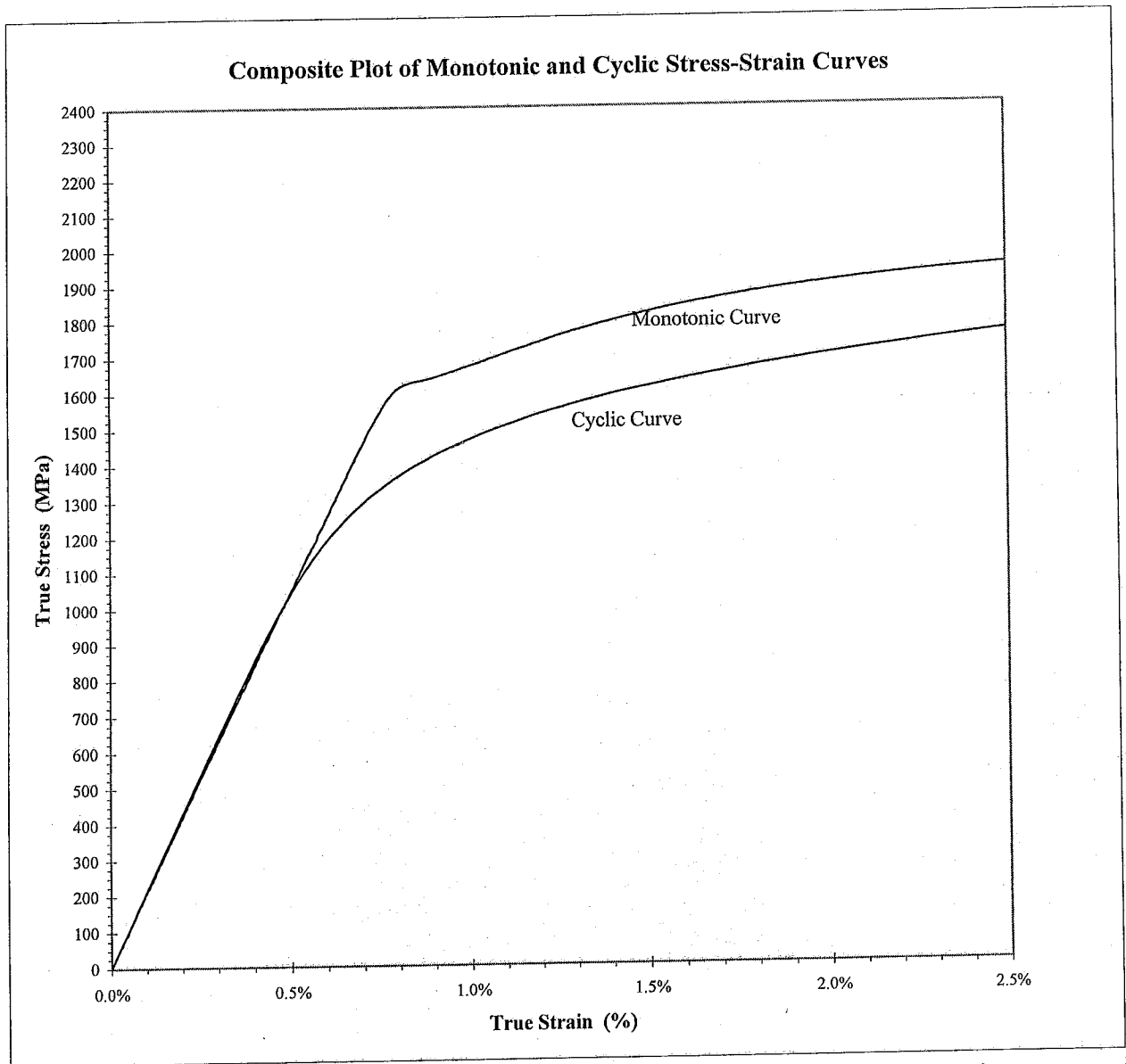Figure 7: True stress amplitude versus true strain amplitude

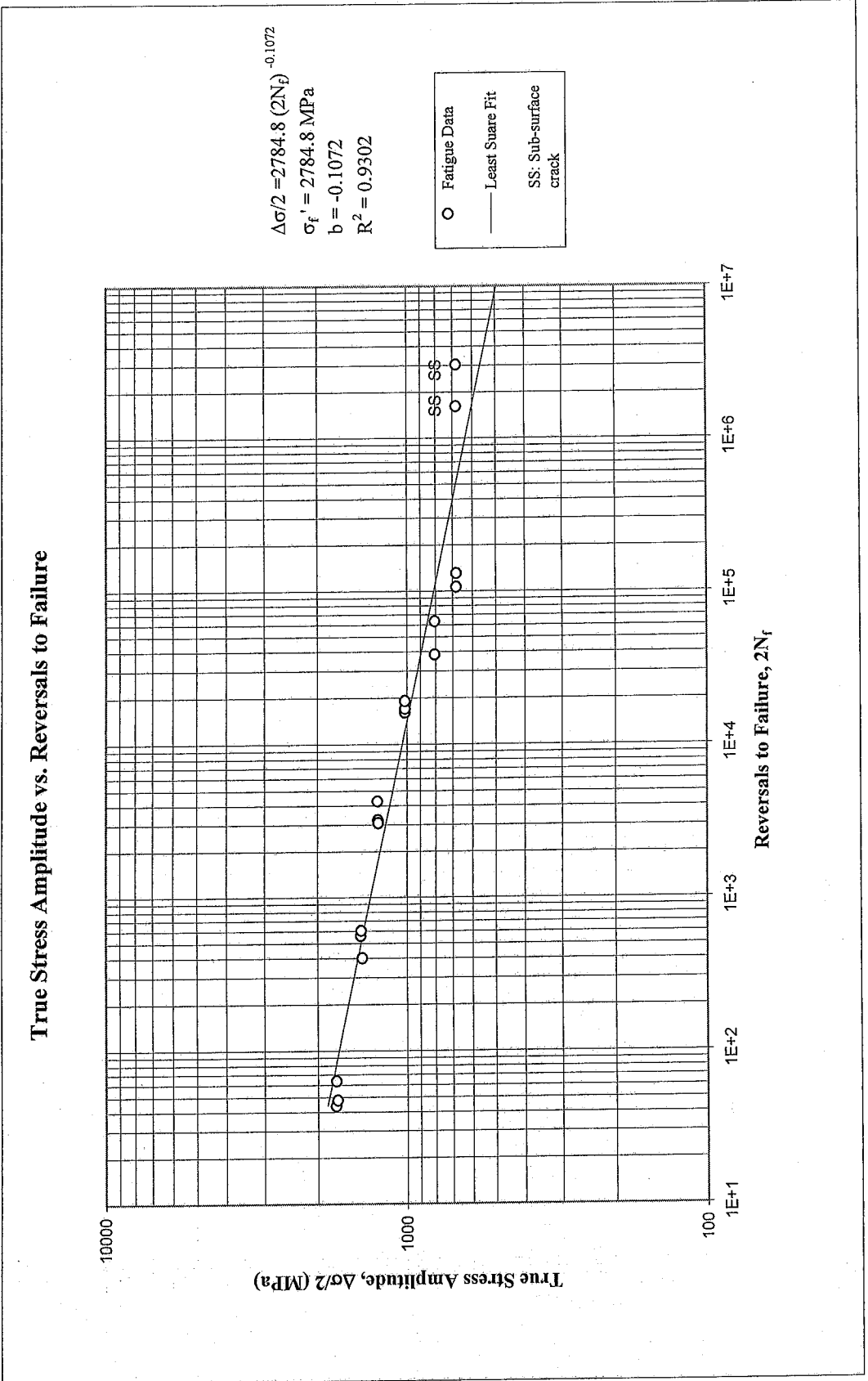**Composite Plot of Monotonic and Cyclic Stress-Strain Curves**

Figure 8: Composite plot of cyclic and monotonic stress-strain curves
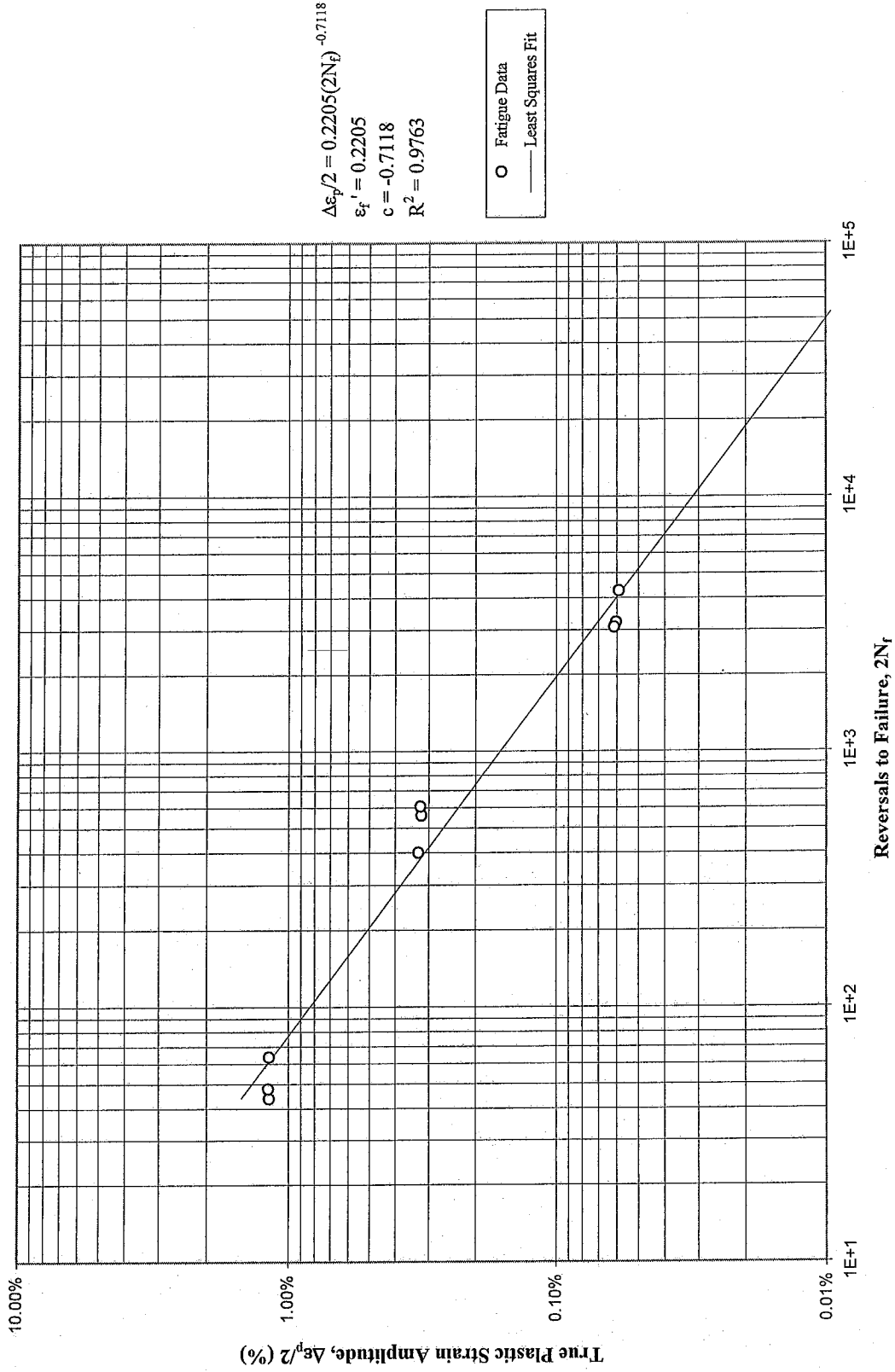
Figure 9: True stress amplitude versus reversals to failure

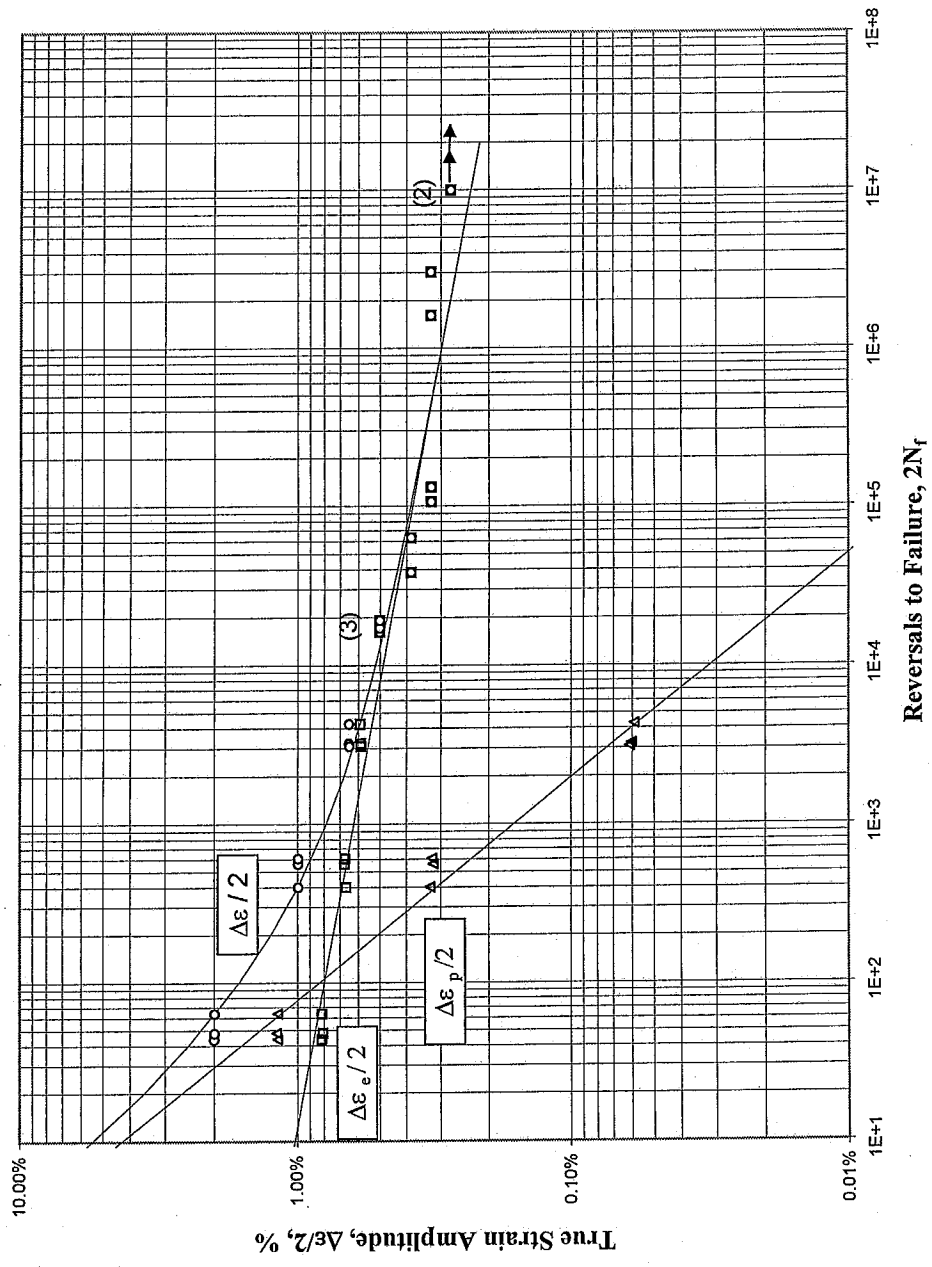Figure 10: Calculated true plastic strain amplitude versus reversals to failure

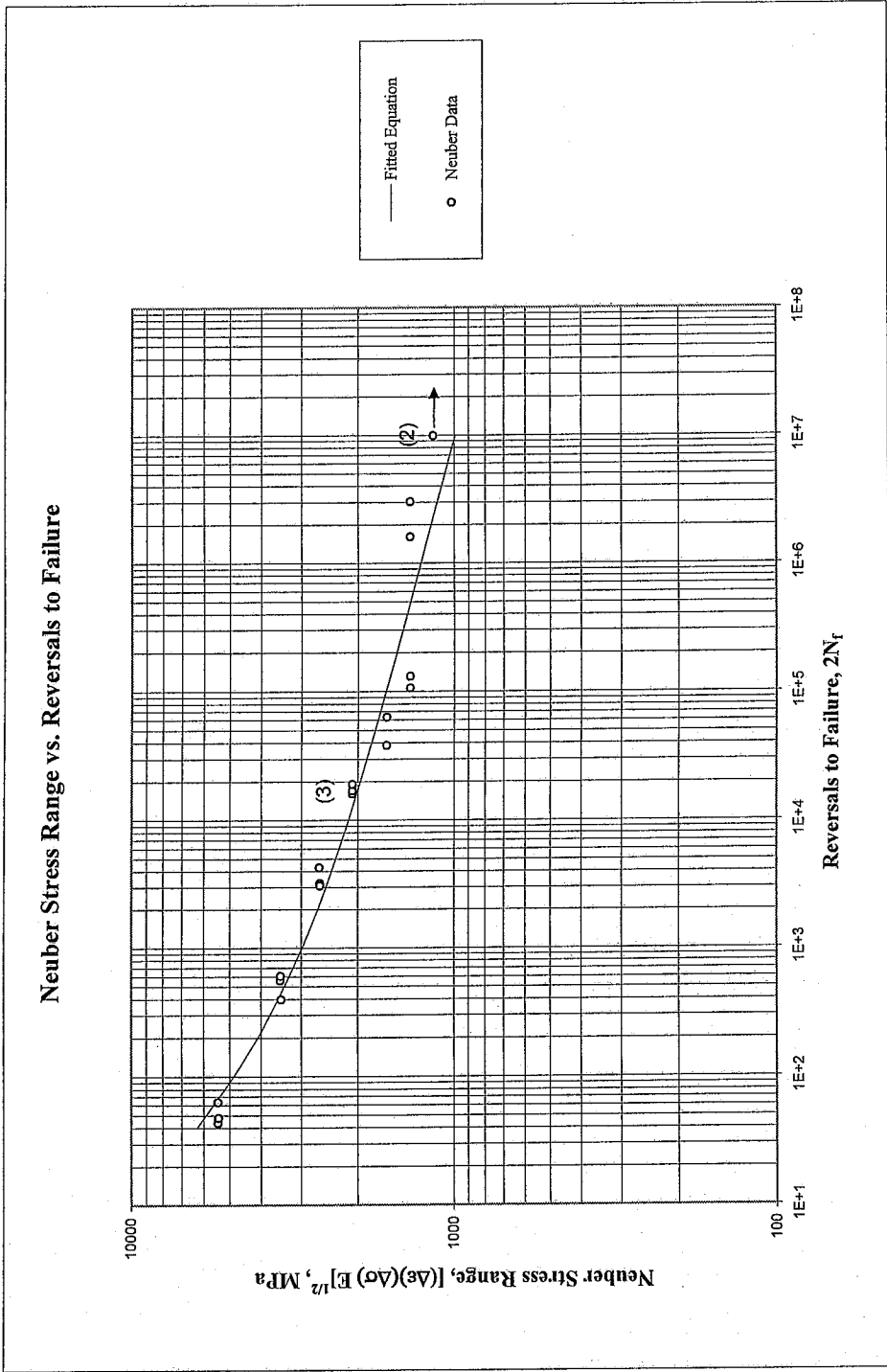Figure 11: True strain amplitude versus reversals to failure

Figure 12: Neuber stress range versus reversals to failure

REFERENCES

[1] ASTM Standard E606-92, "Standard Practice for Strain-Controlled Fatigue Testing," Annual Book of ASTM Standards, Vol. 03.01, 2004, pp. 593-606.

[2] ASTM Standard E83-02, "Standard Practice for Verification and Classification of Extensometers," Annual Book of ASTM Standards, Vol. 03.01, 2004, pp. 232-244.

[3] ASTM Standard E1012-99, "Standard Practice for Verification of Specimen Alignment Under Tensile Loading," Annual Book of ASTM Standards, Vol. 03.01, 2004, pp. 763-770.

[4] ASTM Standard E8-04, "Standard Test Methods for Tension Testing of Metallic Materials," Annual Book of ASTM Standards, Vol. 03.01, 2004, pp. 62-85.

[5] ASTM Standard E112-96, "Standard Test Methods for Determining Average Grain Size," Annual Book of ASTM Standards, Vol. 03.01, 2004, pp. 267-292.

[6] ASTM Standard E45-97, "Standard Test Methods for Determining the Inclusion Content of Steel," Annual Book of ASTM Standards, Vol. 03.01, 2004, pp. 187-199.

[7] ASTM Standard E739-91, "Standard Practice for Statistical Analysis of Linear or Linearized Stress-Life (S-N) and Strain-Life (ε-N) Fatigue Data," Annual Book of ASTM Standards, Vol. 03.01, 1995, pp. 670-676.

[8] ASTM Standard E646-00, "Standard Test Method for Tensile Strain-Hardening Exponents (n-values) of Metallic Sheet Materials," Annual Book of ASTM Standards, Vol. 03.01, 2004, pp. 619-626.

[9] Bridgman, P. W., "Stress Distribution at the Neck of Tension Specimen," *Transactions of American Society for Metals*, Vol. 32, 1944, pp. 553-572.

[10] Stephens R. I., Fatemi A., Stephens R. R. and Fuchs H. O., "*Metal Fatigue in Engineering*", Second edition, Wiley Interscience, 2000.

APPENDIX

Table A.1: Summary of monotonic tensile test results

Specimen ID	Do, mm (in.)	Df, mm (in.)	Lo, mm (in.)	Lf, mm (in.)	E, GPa (ksi)	YS (offset=0.2%), MPa (ksi)	UYS, MPa (ksi)	LYS, MPa (ksi)	YPE, %	Su MPa (ksi)	K, MPa (ksi)	n	%EL, %	%RA, %	R, mm (in.)	σ_f*, MPa (ksi)	ε_f
76-5	5.05 (0.199)	4.39 (0.173)	7.62 (0.30)	8.64 (0.34)	218.8 (31,727.3)	1680.3 (243.7)	-	-	-	1932.7 (280.3)	2,650.1 (384.4)	0.0712	13.3%	24.4%	5.08 (0.200)	1862.8 (295.2)	25.7%
76-25	5.05 (0.199)	4.88 (0.192)	7.62 (0.30)	7.90 (0.31)	207.2 (30,053.7)	1658.1 (240.5)	-	-	-	1916.0 (277.9)	2,601.6 (377.3)	0.0708	3.7%	6.9%	7.62 (0.300)	1855.2 (269.1)	6.9%
Average values					213.0 (30,890.5)	1669.2 (242.1)	-	-	-	1924.3 (279.1)	2,625.9 (380.8)	0.0710	8.5%	15.7%	6.35 (0.250)	1859.0 (282.1)	16.3%

* The values of true fracture strength are corrected for necking according to the Bridgman correction factor.

Table A.2: Summary of constant amplitude completely reversed fatigue test results

Specimen ID	Test control mode	Test freq., Hz	E, GPa (ksi)	At midlife ($N_{50\%}$)							$2N_{50\%}$,[a] reversals	$(2N_f)_{50\%}$,[b] reversals	Failure location [c]
				E', GPa (ksi)	$\Delta\varepsilon/2$, %	$\Delta\varepsilon_p/2$ (calculated), %	$\Delta\varepsilon_p/2$ (measured), %	$\Delta\sigma/2$, MPa (ksi)	σ_m, MPa (ksi)				
76-24	strain	0.20	203.7 (29,545.1)	190.0 (27,560.3)	1.993%	1.179%	1.109%	1735.0 (251.6)	-36.3 (-5.3)	22	44	IGL
76-17	strain	0.20	201.4 (29,215.4)	186.9 (27,109.0)	1.992%	1.187%	1.103%	1715.6 (248.8)	-33.2 (-4.8)	28	48	IGL
76-12	strain	0.20	206.5 (29,947.9)	192.8 (27,968.9)	1.991%	1.177%	1.113%	1733.7 (251.4)	-37.1 (-5.4)	32	64	IGL
76-7	strain	0.20	203.3 (29,486.7)	195.1 (28,291.2)	0.991%	0.319%	0.266%	1432.3 (207.7)	-26.9 (-3.9)	256	562	IGL
76-8	strain	0.20	202.6 (29,385.5)	194.5 (28,209.6)	0.992%	0.327%	0.262%	1415.0 (205.2)	-27.3 (-4.0)	256	402	IGL
76-11	strain	0.20	204.4 (29,639.6)	197.3 (28,610.4)	0.992%	0.322%	0.271%	1426.9 (206.9)	-17.3 (-2.5)	256	608	IGL
76-10	strain	0.50	211.5 (30,669.7)	210.1 (30,467.7)	0.648%	0.060%	0.046%	1250.9 (181.4)	83.6 (12.1)	2,048	3,232	IGL
76-21	strain	0.50	205.0 (29,728.7)	205.6 (29,819.5)	0.648%	0.059%	0.041%	1256.0 (182.2)	-28.2 (-4.1)	2,048	4,286	IGL
76-4	strain	0.50	215.4 (31,246.1)	210.4 (30,517.5)	0.647%	0.061%	0.052%	1247.6 (180.9)	8.5 (1.2)	1,604	3,090	IGL
76-2	strain load	0.50 2.00	201.9 (29,286.3)	- -	0.500%	-	-	1013.9 (147.1)	0.0 (0.0)	8,583	17,166	IGL
76-9	load	2.00	-	- -	0.500%	-	-	1013.9 (147.1)	0.0 (0.0)	8,114	16,228	IGL
76-18	load	2.00	-	- -	0.500%	-	-	1013.9 (147.1)	0.0 (0.0)	9,617	19,234	IGL
76-15	load	4.00	-	- -	0.385%	-	-	804.4 (116.7)	0.0 (0.0)	31,751	63,502	IGL
76-19	load	4.00	-	- -	0.385%	-	-	804.4 (116.7)	0.0 (0.0)	19,229	38,458	IGL
76-16	load	4.00 15.00	-	- -	0.325%	-	-	679.1 (98.5)	0.0 (0.0)	1,525,901	3,051,802	SS
76-23	load	4.00 15.00	-	- -	0.325%	-	-	679.1 (98.5)	0.0 (0.0)	809,439	1,618,878	SS
76-14	load	4.00	-	- -	0.325%	-	-	679.1 (98.5)	0.0 (0.0)	66,000	132,000	IGL
76-22	load	4.00	-	- -	0.325%	-	-	679.1 (98.5)	0.0 (0.0)	53,500	107,000	IGL
76-6	load	20.00	-	- -	0.275%	-	-	574.6 (83.3)	0.0 (0.0)	-	>10,000,000	No Failure
76-1	load	20.00	-	- -	0.275%	-	-	574.6 (83.3)	0.0 (0.0)	-	>10,000,000	No Failure

[a] $2N_{50\%}$ is defined as the midlife reversal

[b] $2(N_f)_{50\%}$ is defined as reversal of 50% load drop or failure

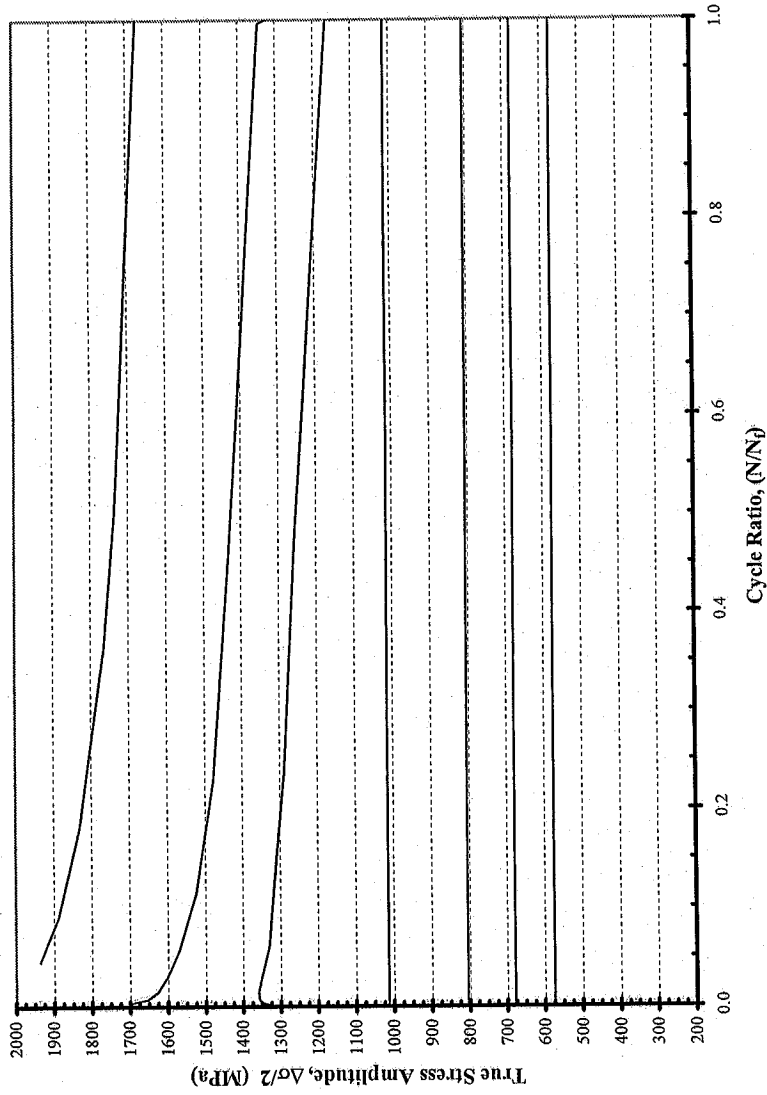[c] IGL = inside gage length;   SS: Subsurface cracking

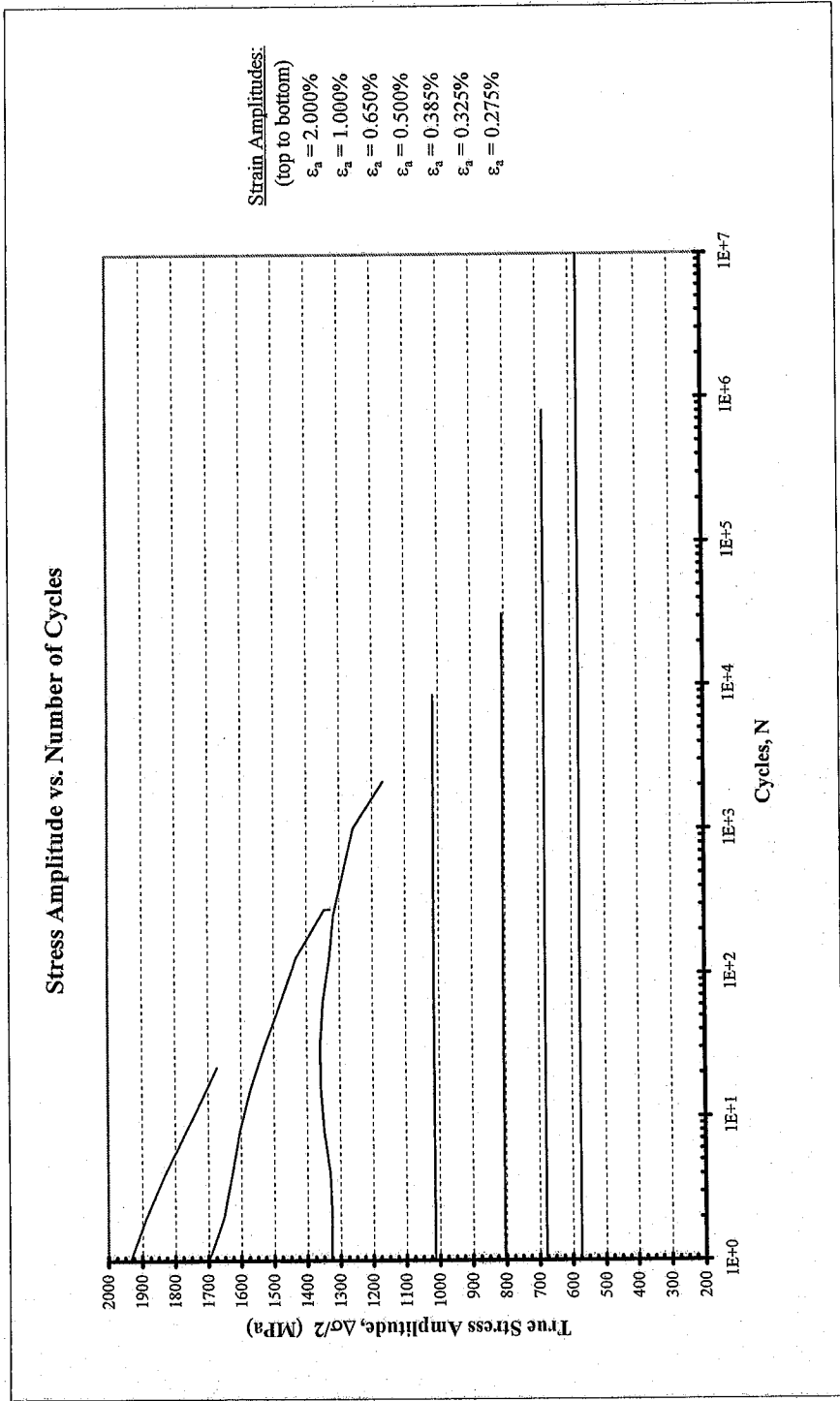Figure A.1a: True stress amplitude versus normalized number of cycles
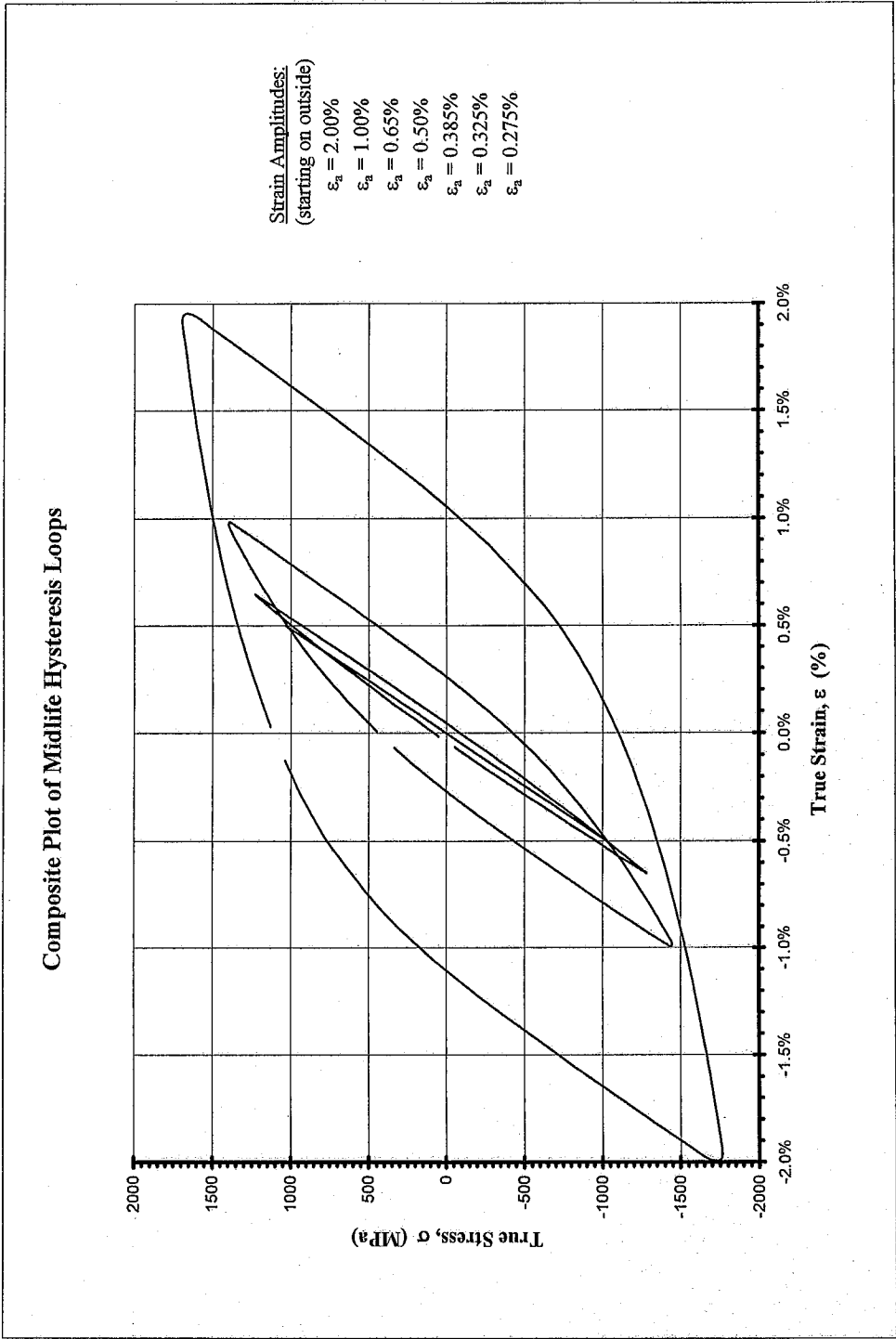
Figure A.1b: True stress amplitude versus number of cycles

Figure A.2: Composite plot of midlife hysteresis loops